Positron Annihilation Lifetime Spectroscopy of Poly(ethylene terephthalate): Contributions from Rigid and Mobile Amorphous Fractions

Brian G. Olson,† Jun Lin,‡ Sergei Nazarenko,‡ and Alexander M. Jamieson*,‡

Department of Macromolecular Science and Engineering, and Department of Physics, Case Western Reserve University, Cleveland, Ohio 44106

Received June 16, 2003; Revised Manuscript Received August 11, 2003

ABSTRACT: Systematic divergences in the orthopositronium (o-Ps) annihilation lifetimes, τ_3, and intensities, I_3, are observed, when comparing melt-crystallized and cold-crystallized poly(ethylene terephthalate) (PET) as a function of crystallinity. Following a previous analysis of corresponding deviations in oxygen permeability, the divergences in I_3 and τ_3 are traced to distinct characteristic values for the probability of o-Ps formation and o-Ps lifetime in the rigid amorphous phase (RAF) associated with the crystalline lamellae and the mobile amorphous regions (MAF) which are unperturbed by the presence of the crystal phase. Utilizing independent information on the volume fractions of RAF and MAF, a quantitative analysis of the o-Ps annihilation parameters is possible.

Introduction

Positron annihilation lifetime spectroscopy (PALS) is a useful probe to characterize structural disorder in polymers.[1] In particular, quantitative comparisons have been established[2] between the characteristic parameters, intensity I_3 and lifetime τ_3 of the orthopositronium annihilation component of PALS and fractional free volume f_v of amorphous polymers, as computed via statistical mechanical theory.[3] Specifically, I_3, which characterizes the probability of o-Ps formation, is a measure of the density of free volume holes, and τ_3 can be related to the hole radius R and hence to the hole volume $v_f = (4\pi/3)R^3$. Thus, $f_v = CI_3v_f$, where C is a constant which must be established for each polymer. In applying this relationship, care has to be taken to avoid anomalous changes in I_3, which arise due to radiation damage in the polymer.[4−6] Alternative approaches to correlate o-Ps lifetimes and fractional free volume, which avoid the use of I_3 data, have been described and successfully tested.[7−10]

PALS studies of semicrystalline polymers have been reported.[11−21] In one such study,[11] on poly(ether ether ketone) (PEEK), it was observed that the o-Ps intensity, I_3, decreases linearly with the degree of crystallinity. This is consistent with the expectation that o-Ps forms only in the amorphous phase and not in the more dense crystal phase. For several other polymers, notably polyethylene[12−14] and poly(tetrafluoroethylene),[16,17] two long-lived o-Ps components have been reported: one assigned to o-Ps annihilation in the chain-folded regions and the other to annihilation in the amorphous phase. In other polymers, a single o-Ps component is observed, but the linear proportionality between I_3 and % crystallinity fails. One such example concerns syndiotactic polystyrene,[21] whose crystal density is in fact smaller than that of the amorphous phase. Here, detailed analysis of the PALS data suggests that o-Ps forms in open linear channels, which exist in the crystal structure, and then diffuses rapidly into the amorphous phase, where annihilation occurs. A second example is poly(ethylene terephthalate) (PET).[15] Here, I_3 decreases linearly with the degree of crystallinity, but the decrease cannot be fully accounted for, if one assumes o-Ps localizes only in the amorphous phase. It was concluded that o-Ps again forms in both the amorphous and crystal phases but that the two lifetimes are so close a single o-Ps component, with a weighted average lifetime and intensity, are determined by the PALS fit.

This paper is prompted by a recent study[22] of oxygen permeability in semicrystalline PET at room temperature, which investigated the well-established observation[23] that the gas solubility is reduced, but not in direct proportion with the decrease in amorphous volume. The study demonstrated that the O_2 solubility in melt-crystallized PET is higher than in cold-crystallized PET.[22] This recent work[22] further established that the observed decreases in solubility and diffusion coefficient of oxygen in semicrystalline PET could be explained by the three-phase model[24−26] of semicrystalline polymers in which a third phase or fraction, termed the rigid amorphous fraction (RAF), is considered in addition to the crystalline phase and the normal or mobile amorphous fraction (MAF). The RAF refers to the thin amorphous layers between crystal lamellae, where the molecular mobility of the chains is restricted in comparison to the normal amorphous phase. The unusually high gas solubility in semicrystalline PET is therefore ascribed to the formation of RAF, which vitrifies at a temperature much higher than T_g, and thus develops a higher free volume on cooling.[22,27,28] Analysis of the heat capacity jump at T_g, specific volume, and % crystallinity of melt-crystallized and cold-crystallized PET specimens yields data on the volume fractions of RAF, MAF, and crystal phases and permits a quantitative treatment of the oxygen solubility of each specimen.[22] The results indicate that, while the volume fraction of RAF in melt-crystallized PET is smaller than that in cold-crystallized PET, the specific volume and hence the fractional free volume are much higher because of the higher effective

† Department of Physics.
‡ Department of Macromolecular Science and Engineering.
* To whom correspondence should be addressed. E-mail: amj@cwru.edu.

10.1021/ma034813u CCC: $25.00
Published on Web 09/12/2003

vitrification temperature. This enhanced free volume is the origin of the higher oxygen solubility of melt-crystallized PET vs cold-crystallized PET.[22]

In an analogous procedure, we here describe a PALS study of the same series of melt-crystallized and cold-crystallized PET specimens, each of which have been thoroughly characterized with respect to degree of crystallinity and specific volume. The aim is to confirm the existence of enhanced free volume of RAF in melt-crystallized PET and to demonstrate that a self-consistent treatment of the o-Ps annihilation data can be achieved within the three-phase model.

Experimental Section

Sample Preparation. PET with 2.6 mol % of isophthalic acid (PET-I/2.6), typical commercial PET bottle grade (PET-80), was supplied as pellets by KoSa Corp., Spartanburg, SC. After being dried in vacuo at 120 °C for 24 h, the pellets were placed in the 6 × 6 in. cavity of a 200 μm thick spacer and sandwiched between two 8 × 8 in. polished steel platens covered with Teflon-coated aluminum foil. To prepare amorphous PET plaques, the platens were first placed in a press preheated at 270 °C and held for 5 min without pressure. The pressure was then increased to 20 000 psi and, subsequently, released. This cycle was repeated three times to remove the air bubbles from the compression-molded plaques. Finally, the platens were held at 20 000 psi for 5 min and quenched into an ice−water mixture.

For cold crystallization, the amorphous plaques were first sealed into aluminum foil and annealed in an oil bath at 110 °C, for various times, and finally quenched into an ice−water mixture. For isothermal melt crystallization, plaques were first compression-molded at 270 °C, as described previously, and then the platens with a sample between were rapidly transferred to a convection oven which was preset at crystallization temperature T_c = 210 °C. In the oven, the samples were crystallized for various times. After crystallization was completed, the samples were quenched into an ice−water mixture.

Sample Characterization. Glass transition, melting, and crystallization behavior of PET were measured using a Perkin-Elmer DSC-7 and Rheometric Scientific SP DSC. The calibration was carried out using indium, tin, and sapphire standards. A heating rate of 10 °C/min was used over the whole studied temperature range.

Density was measured using a gradient column constructed from a solution of calcium nitrate/water in accordance with ASTM-D 1505 method B. The column was calibrated with glass floats of known density. Small pieces from each plaque (~25 mm^2) were placed in the column and allowed to equilibrate for 15 min before a measurement was taken.

Positron Annihilation Lifetime Spectroscopy. The positron annihilation lifetime spectroscopy (PALS) experiments were conducted with a fast−fast coincidence system, described in previous work,[29−31] having a time resolution of 220 ps. From each sample plaque, 10 pieces where cut, each of 1 × 1 cm^2 area. On each side of a 30 μCi ^{22}Na positron source, five pieces of the sample were stacked, for a 1 mm total thickness. All measurements were taken over an hour, for a total of 1 × 10^6 counts in each PALS spectra. Temperature measurements where taken by first decreasing the temperature to −60 °C and waiting for an hour to allow for equilibrium before the experiment began. The temperature was then sequentially increased in 10 °C steps, collecting a spectrum each step, after waiting 10 min to allow for equilibrium.

To verify that the stacking of the sample does not result in a modification of the measured PALS parameters, a 1.5 mm thick amorphous PET sample was prepared following the same procedure as that for the thin samples. No difference in the PALS parameters was detected between the stacked and 1.5 mm thick sample.

To check for any radiation effects,[4−6] an amorphous PET and a 24.9% crystalline melt-crystallized sample were each analyzed at 23 °C over a period of 24 h, collecting a PALS spectrum each hour. All PALS parameters remained constant over the 24 h period for each sample. To further explore the possibility of radiation effects, a temperature cycling experiment on the amorphous PET sample was performed. The temperature was first increased in 10 °C intervals from 30 to 90 °C, below the point at which cold crystallization can occur, taking a spectrum at each interval. The temperature was then decreased from 90 to 30 °C, again, taking a spectrum every 10 °C. Finally, the temperature was again increased from 30 to 90 °C, collecting spectra every 10 °C. At each temperature, no difference in the PALS parameters was detected between the first heating, first cooling, and second heating cycle.

The PALS spectra were tested against three- and four-component fits using the PATFIT software package.[32] Optimal fits were obtained to three components with variances smaller than 1.1. The free volume hole radius, R, was calculated from the o-Ps lifetime, τ_3, using the semiempirical equation[33,34]

$$\tau_3 = \frac{1}{2}\left[1 - \frac{R}{R+\Delta R} + \frac{1}{2\pi}\sin\left(\frac{2\pi R}{R+\Delta R}\right)\right]^{-1} \quad \text{(ns)} \qquad (1)$$

where ΔR has been empirically determined to be ΔR = 0.1656 nm by fitting eq 1 to o-Ps annihilation data for molecular solids of known pore sizes.

Table 1. Specific Volume and Volume Fractions of Crystalline, Mobile Amorphous, and Rigid Amorphous Phases of Samples Studied

specific vol (cm^3/g)	ϕ_c	ϕ_{MAF}	ϕ_{RAF}
0.7473	0.000	1.000	0.000
	Melt-Crystallized at 210 °C		
0.7450	0.053	0.962	−0.015
0.7449	0.066	0.953	−0.019
0.7382	0.105	0.841	0.054
0.7360	0.143	0.809	0.048
0.7323	0.203	0.654	0.143
0.7338	0.228	0.649	0.123
0.7317	0.244	0.604	0.152
0.7288	0.249	0.660	0.091
0.7245	0.325	0.493	0.182
0.7224	0.331	0.517	0.152
	Cold-Crystallized at 110 °C		
0.7419	0.069	0.892	0.038
0.7419	0.071	0.865	0.064
0.7413	0.071	0.884	0.045
0.7417	0.077	0.902	0.022
0.7384	0.131	0.772	0.096
0.7355	0.184	0.623	0.193
0.7299	0.232	0.449	0.320
0.7293	0.242	0.389	0.369
0.7293	0.257	0.396	0.347
0.7292	0.247	0.421	0.332

Results and Discussion

Specimens of cold-crystallized PET (T_c = 110 °C) and melt-crystallized PET (T_c = 210 °C) were prepared with varying crystallinities.[22] The properties of these samples have been thoroughly documented in a previous paper[22] by methods outlined in the Experimental Section. In Table 1, for each specimen, we summarize the results on specific volume, % crystallinity, and the volume fractions of the crystal phase, ϕ_c, and MAF, ϕ_{MAF}. Also listed in Table 1 are values of the volume fraction of RAF, computed from the relation $\phi_{RAF} = 1 - \phi_c - \phi_{MAF}$. In parts a and b of Figure 1, we plot for melt- and cold-crystallized samples, respectively, ϕ_{MAF} and ϕ_{RAF} vs ϕ_c. The straight line in each figure indicates the total amount of amorphous phase. Evidently, ϕ_{RAF} increases and ϕ_{MAF} decreases with degree of crystallinity, and for a specified ϕ_c, cold-crystallized specimens have a higher ϕ_{RAF} than melt-crystallized. This can be rationalized if lower crystallization temperatures result in thinner

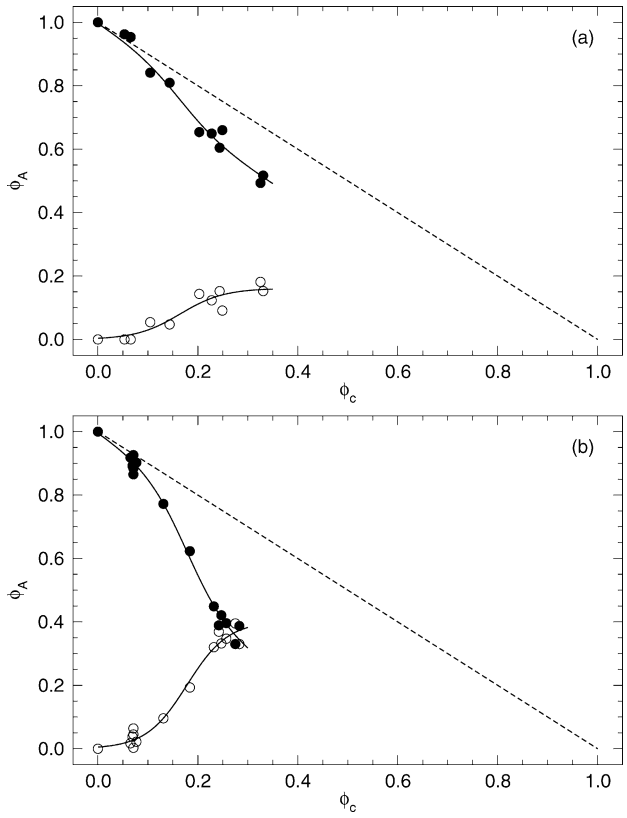

Figure 1. Volume fractions of MAF (●) and RAF (○) as a function of crystallinity for (a) amorphous PET melt-crystallized at 210 °C for various times and (b) amorphous PET cold-crystallized at 110 °C for various times. Solids lines are to help guide the eye, and the dashed lines represent the standard two-phase model.

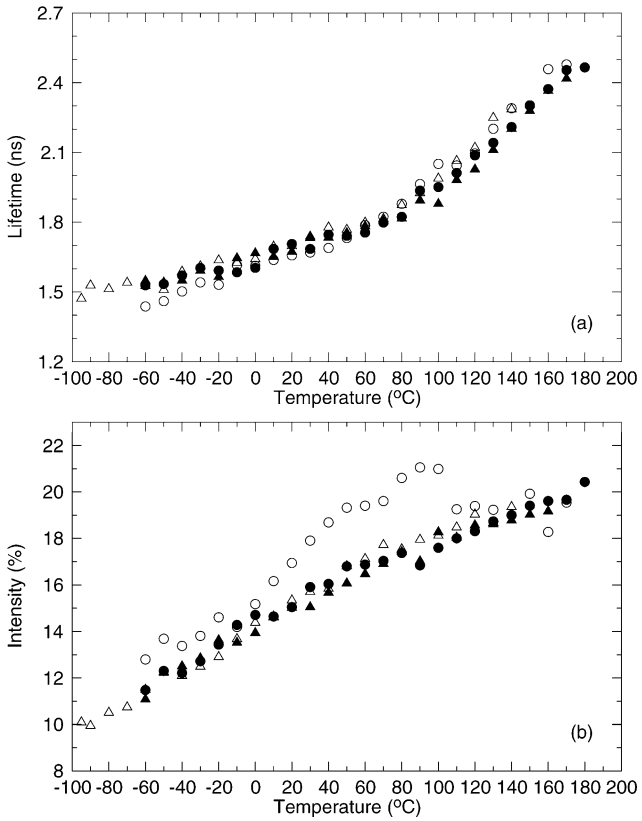

Figure 2. Orthopositronium lifetime (a) and intensity (b) for amorphous PET (○), second run of amorphous PET (●), amorphous PET annealed at 160 °C for 2 h (△), and amorphous PET annealed at 180 °C for 2 h (▲).

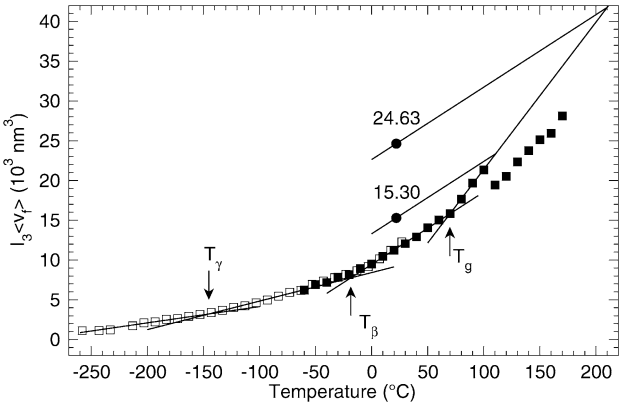

Figure 3. Temperature dependence of $I_3 v_f$ for amorphous PET (■), including low-temperature values from Wang et al.[20] (□).

lamellae, so that the number of lamellae increases for a specified crystallinity, leading to a larger amount of constrained, interlamellar amorphous phase.[22]

In parts a and b of Figure 2, we show the temperature dependence of τ_3 and I_3, respectively, for an amorphous PET specimen, rapidly quenched from the melt, and compare this with three other data sets—one from a second heating scan of the amorphous sample and two others after annealing the sample for 2 h at 160 and 180 °C, respectively. As evident in Figure 2a, τ_3 increases with temperature, indicating the expansion of hole size on heating. In addition, as expected, a distinct increase in the temperature coefficient of τ_3 is observed at the glass transition temperature, $T_g \sim 80$ °C, which reflects that the thermal expansion of hole volume above T_g is greater than below T_g. No apparent differences are observed when comparing the first heating scan vs the later heating scans. Figure 2b shows that I_3 increases substantially with temperature and shows a sudden decrease at $T \sim 100$ °C, which reflects the onset of cold crystallization in the material. The I_3 values in the second heating scan decrease relative to the first scan but also increase with temperature, though not so strongly. The I_3 values of the third and fourth heating scans do not appear to be significantly different from the second scan. Here, we note that our values of τ_3 and I_3 are numerically quite consistent with literature data.[15,18−20] The strong temperature dependence of I_3 is interesting because it contrasts with the relatively weak T dependence of I_3 in purely amorphous polymers like atactic polystyrene. The behavior of I_3 is more reminiscent of liquid crystalline polymers[35] and indicates that a significant contribution to the increase of free volume with temperature, as probed by o-Ps annihilation, comes from the creation of holes accessible to o-Ps formation as well as from hole expansion. In Figure 3, for amorphous PET, we show the temperature dependence of the quantity $I_3 v_f$, which is proportional to fractional free volume, with v_f calculated from τ_3 via eq 1. Here we have included values calculated from data of Wang et al.[20] after shifting their I_3 values vertically by −2.1 to match our data at 20 °C. Their results extend to lower temperatures than pursued in our experiments and evidently are in good agreement with our observations. In Figure 3, in addition to T_g, we have indicated locations of the sub-glass transitions, T_β and T_γ, identified by Wang et al.[20]

In Figure 4a,b, we show the dependence of τ_3 and I_3 on degree of crystallinity, and in Figure 5, we display

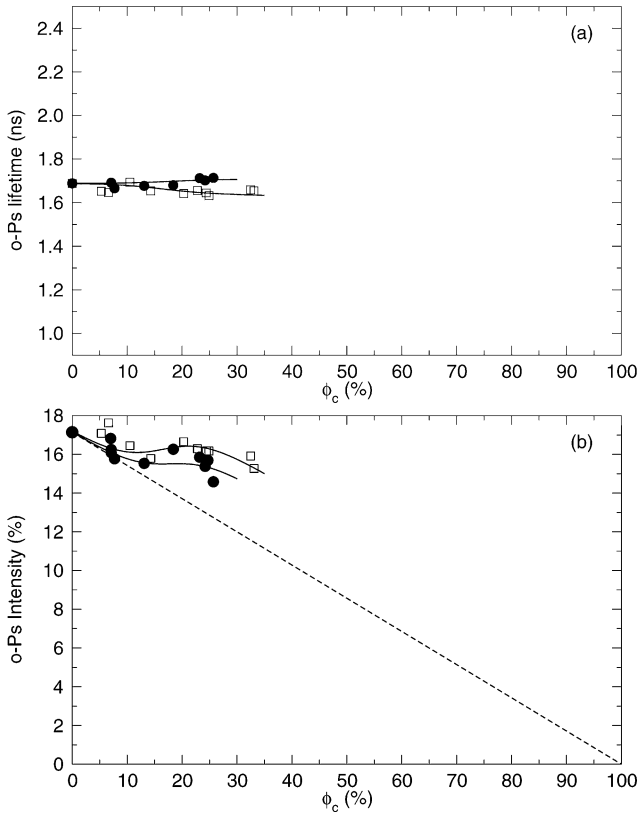

Figure 4. Dependence of orthopositronium lifetime (a) and intensity (b) on volume fraction of crystallinity for melt-crystallized (□) and cold-crystallized (●) PET. Dashed line represents the two-phase model, and the solid lines are generated as described in the text.

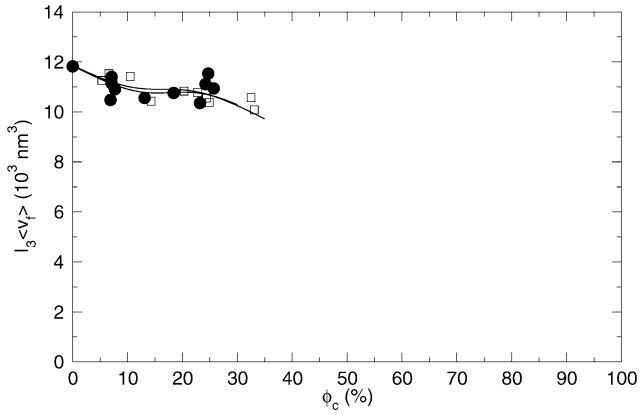

Figure 5. Dependence of free volume, as measured by PALS, on volume fraction of crystallinity for melt-crystallized (□) and cold-crystallized (●) PET.

the corresponding behavior of the product $I_3 v_f$, where v_f is computed from τ_3 via eq 1. Small differences are observed when comparing cold-crystallized vs melt-crystallized. As evident in Figure 4a,b, cold-crystallized specimens exhibit a larger τ_3, and smaller I_3, for a specified degree of crystallinity. However, as seen in Figure 5, when computing the fractional free volume, $I_3 v_f$, the variations in I_3 and τ_3 (hence v_f) compensate, so that $I_3 v_f$ shows no statistically significant differences, when comparing cold-crystallized and melt-crystallized specimens.

It is interesting to note certain analogies between the present PALS data and the earlier study of O_2 permeability.[22] There, it was observed that, in the melt-crystallized specimens, O_2 solubility, S, was higher but

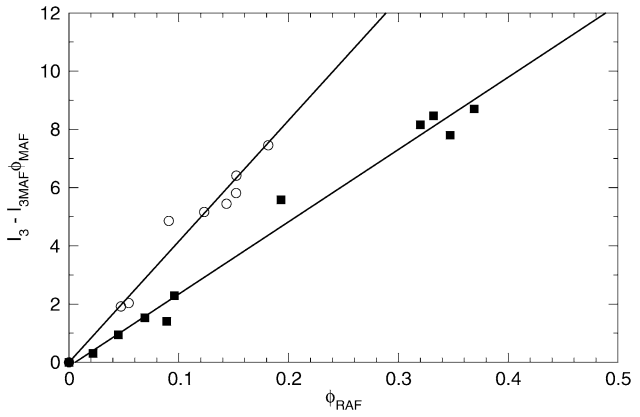

Figure 6. Determination of I_{3RAF}, using eq 2, for melt-crystallized (○) and cold-crystallized (■) PET.

the O_2 diffusion coefficients, D, were smaller compared to those of cold-crystallized. These differences compensated so that the permeability, $P = SD$, showed no significant differences between the two types of materials. Contrasting these observations with the PALS results summarized in Figures 4 and 5 suggests that the dominant free volume parameter, which controls the diffusion process, is the hole volume, whereas the dominant parameter controlling the solubility is the hole density.

To proceed further, we need to individually characterize the PALS contributions from RAF and MAF. We assume that o-Ps formation occurs only in the amorphous phase and that the o-Ps lifetime and intensity of the mobile amorphous phase, I_{3MAF} and τ_{3MAF}, are those measured for amorphous PET (Figure 2). We have the following relationships:

$$I_3 = \phi_{MAF} I_{3MAF} + \phi_{RAF} I_{3RAF} \tag{2}$$

and

$$\tau_3 = \frac{\phi_{MAF} I_{3MAF} \tau_{3MAF} + \phi_{RAF} I_{3RAF} \tau_{3RAF}}{\phi_{MAF} I_{3MAF} + \phi_{RAF} I_{3RAF}} \tag{3}$$

Hence

$$I_3 \tau_3 = \phi_{MAF} I_{3MAF} \tau_{3MAF} + \phi_{RAF} I_{3RAF} \tau_{3RAF} \tag{4}$$

Next, we recall that the product $I_3 v_f$ is proportional to the fractional free volume. It appears reasonable to assume that the proportionality constant for RAF is the same as for MAF. It then follows that the following additional relationship can be expressed:

$$I_3 v_f = \phi_{MAF} I_{3MAF} v_{fMAF} + \phi_{RAF} I_{3RAF} v_{fRAF} \tag{5}$$

From these relations, I_{3RAF}, τ_{3RAF}, and v_{fRAF} can be extracted from the slopes of plots of $I_3 - \phi_{MAF} I_{3MAF}$ vs ϕ_{RAF}, $I_3 \tau_3 - \phi_{MAF} I_{3MAF} \tau_{3MAF}$ vs ϕ_{RAF}, and $I_3 v_f - \phi_{MAF} I_{3MAF} v_{fMAF}$ vs ϕ_{RAF}, respectively. Such plots are shown in Figures 6, 7, and 8 and lead to the values summarized in Table 3. As a self-consistency check, the solid lines in Figures 4 and 5 show the values of τ_3, I_3, and $I_3 v_f$ for melt-crystallized and cold-crystallized PET computed from the values in Table 3. These lines accurately depict the small differences observed in the PALS spectra for the two materials. Note that the difference between τ_{3MAF} (Table 2) and τ_{3RAF} (Table 3) is relatively small. Attempts to resolve these differences

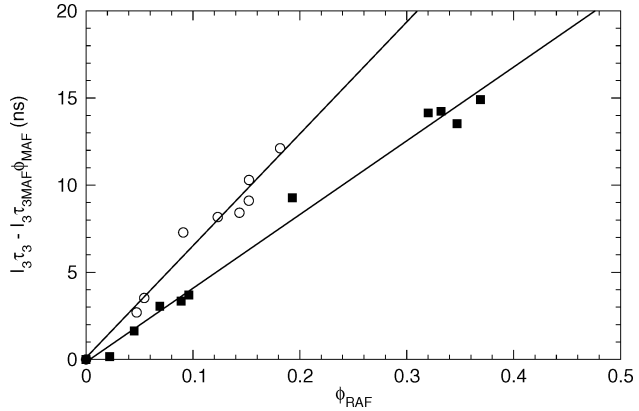

Figure 7. Determination of $I_{3RAF}\tau_{3RAF}$, using eq 4, for melt-crystallized (○) and cold-crystallized (■) PET.

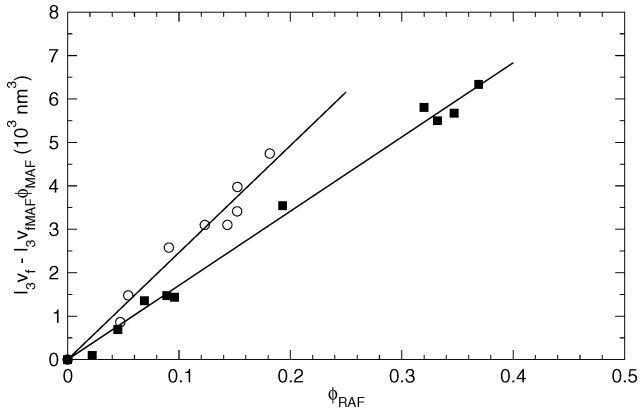

Figure 8. Determination of $I_{3RAF}v_{fRAF}$, using eq 5, for melt-crystallized (○) and cold-crystallized (■) PET.

Table 2. PALS Parameters for the Mobile Amorphous Phase of PET

method	I_{3MAF} (%)	τ_{3MAF} (% ns)	$I_{3MAF}v_{fMAF}$ (Å^3)
amorphous	17.14	1.688	11.88

Table 3. PALS Parameters for the Rigid Amorphous Phases of Cold- and Melt-Crystallized PET

method	I_{3RAF} (%)	$I_{3RAF}\tau_{3RAF}$ (% ns)	$I_{3RAF}v_{fRAF}$ (Å^3)	$I_{3RAF}v_{fRAF}$[a] (Å^3)	τ_{3RAF}[b] (ns)	τ_{3RAF}[c] (ns)
cold	24.33	41.78	17.09	15.30	1.717	1.703
melt	41.55	64.95	24.64	24.63	1.563	1.572

[a] Determined from extrapolation to room temperature from the crystallization temperature using Figure 3. [b] Calculated from $I_{3RAF}\tau_{3RAF}/I_{3RAF}$. [c] Calculated from $I_{3RAF}v_{fRAF}/I_{3RAF}$ and eq 1.

through four-component fits to the PALS data were unsuccessful.

These results are a quantitative documentation of the increased free volume in the RAF. The fractional free volume of the melt-crystallized RAF, as measured by the product $I_{3RAF}v_{fRAF}$ (24.64), is larger than that of cold-crystallized RAF (17.09), which is in turn larger than that of the MAF (11.82). This observation is qualitatively consistent with corresponding changes in specific volume of RAF deduced in previous work, which found, for melt- and cold-crystallized RAF, $V_{sp} = 0.781$ and 0.754 cm^3/g, respectively, while MAF has a specific volume of 0.749 cm^3/g. Another interesting finding from Table 3 is that the structures of the RAF in melt-crystallized and cold-crystallized PET, as depicted by the individual values of τ_3 and I_3, are substantially different. Melt-crystallized has a larger hole density and small average hole volume; cold-crystallized has a smaller hole density and larger average hole size. These differences apparently correlate to the observations of higher O_2 solubility and smaller O_2 diffusion coefficient in melt-crystallized; cf. cold-crystallized PET.[22] A measure of support for this analysis of o-Ps annihilation in three-phase semicrystalline PET is provided by the further observation that the o-Ps fractional free volumes are numerically consistent with values estimated from specific volumes of MAF and RAF for melt- and cold-crystallized PET and the Bondi specific volume[36] of PET ($V_w = 0.491$ cm^3/g) according to the equation

$$CI_3v_f = \frac{V_{sp} - KV_w}{V_{sp}} \tag{6}$$

with $C = 3.39 \times 10^{-3}$ and $K = 1.46$. The latter is consistent with the value of 1.39 obtained from Simha and Carri.[37]

Finally, it may be speculated that the free volume parameters of RAF have some relationship to the melt at the crystallization temperature, where its vitrification occurs. To test this, we estimate the values of the product $I_{3RAF}v_{fRAF}$, obtained after cooling from the respective crystallization temperatures to room temperature, by the graphical constructs shown in Figure 3. Here we have assumed, following Lin et al.,[22] that the coefficient of thermal expansion of fractional free volume of RAF is the same as that of the normal glass. We obtain values of 24.63 and 15.30 for the melt- and cold-crystallized RAF, respectively. The result for melt-crystallized RAF is remarkably similar to the value obtained from the analysis of Figures 6−8 (Table 3); the predicted cold-crystallized value is 10% smaller. This small deviation may be a result of subtle differences in thermal histories among the cold-crystallized samples. Thus, it appears that the fractional free volume of RAF, as measured by $I_{3RAF}v_{fRAF}$, has some memory of the equilibrium melt at the crystallization temperature, although the structure of RAF, as characterized by the individual values of I_{3RAF} and v_{fRAF}, varies with crystallization temperature.

Conclusions

PALS analysis indicates small but significant differences in the free volume characteristics of cold-crystallized and melt-crystallized PET. These differences can be interpreted self-consistently within the three-phase model, which considers a rigid amorphous fraction associated with the chain segments trapped between crystal lamellae at the crystallization temperature, in addition to the normal mobile amorphous fraction. By utilizing information on the volume fraction of the MAF and RAF, derived from DSC and specific volume measurements, the individual free volume characteristics of the RAF and MAF can be elucidated. The results indicate that the fractional free volume of RAF, as measured by the product of the hole number density and the average hole volume, is related to that of the equilibrium melt at the crystallization temperature but that the structure of RAF, as measured by the individual values of hole number density and average hole volume, is quite different for melt-crystallized vs cold-crystallized samples.

Correlations between PALS and O_2 diffusion parameters suggest that the dominant free volume parameter which controls the diffusion process is the hole volume,

whereas the dominant parameter controlling the solubility is the hole density.

Acknowledgment. The authors are grateful to the National Science foundation for support of this work through Awards DMR-0080114 and DMR-9986467.

References and Notes

(1) Pethrick, R. A. *Prog. Polym. Sci.* **1997**, *22*, 1.
(2) Yu, Z.; Yashi, U.; McGervey, J. D.; Jamieson, A. M.; Simha, R. *J. Polym. Sci., Polym. Phys.* **1996**, *33*, 2295.
(3) Simha, R.; Somcynsky, T. *Macromolecules* **1969**, *2*, 342.
(4) Welander, M.; Maurer, F. H. K. *Mater. Sci. Forum* **1992**, *105*−*110*, 1814.
(5) Li, X. S.; Boyce, M. C. *J. Polym. Sci., Part B* **1993**, *31*, 869.
(6) Peng, Z. L.; Olson, B. G.; McGervey, J. D.; Jamieson, A. M. *Polymer* **1999**, *40*, 3033.
(7) Dlubek, G.; Stejny, J.; Alam, M. A. *Macromolecules* **1998**, *31*, 4574.
(8) Srithawatpong, R.; Peng, Z. L.; Olson, B. G.; Jamieson, A. M.; Simha, R.; McGervey, J. D.; Maier, T. R.; Halasa, A. F.; Ishida, H. *J. Polym. Sci., Part B* **1999**, *37*, 2754.
(9) Schmidt, M.; Maurer, F. H. J. *Polymer* **2000**, *41*, 8419.
(10) Dlubek, G.; Bamford, D.; Rodriguez-Gonzalez, A.; Bornemann, S.; Stejny, J.; Schade, B.; Alam, M. A.; Arnold, M. *J. Polym. Sci., Part B* **2002**, *40*, 434.
(11) Nakanishi, H.; Jean, Y. C. *Macromolecules* **1991**, *24*, 6618.
(12) Dlubek, G.; Stejny, J.; Lupke, T.; Bamford, D.; Petters, K.; Hubner, C.; Alam, M. A.; Hill, M. J. *J. Polym. Sci., Part B* **2002**, *40*, 65.
(13) Brauer, G.; Hertle, W.; Balogh, A. G. *Phys. Status Solidi A* **1988**, *105*, K7.
(14) Kindl, P.; Reiter, G. *Phys. Status Solidi A* **1987**, *104*, 707.
(15) Xie, L.; Gidley, D.; Hristov, H.; Yee, A. *Polymer* **1994**, *35*, 14.
(16) Dlubek, G.; Saarinen, K.; Fretwell, H. M. *Nucl. Instrum. Methods Phys. Res. Sect. B* **1998**, *142*, 139.
(17) Kindl, P.; Puff, W.; Sormann, H. *Phys. Status Solidi A* **1980**, *58*, 489.
(18) Lopez-Castanenes, R.; Angeles, E.; Sanchez, V.; Fendler, J. H. *J. Appl. Polym. Sci.* **1996**, *62*, 451.
(19) Mohamed, H.; Ito, Y.; Imai, M. *J. Chem. Phys.* **1996**, *105*, 4841.
(20) Wang, B.; Wang, Z.; Zhang, M.; Liu, W.; Wang, S. *Macromolecules* **2002**, *35*, 3993.
(21) Olson, B. G.; Prodpran, T.; Jamieson, A. M.; Nazarenko, S. *Polymer* **2002**, *43*, 6775.
(22) Lin, J.; Shenogin, S.; Nazarenko, S. *Polymer* **2002**, *43*, 4733.
(23) Michaels, A. S.; Vieth, W. R.; Barrie, J. *J. Appl. Phys.* **1963**, *34*, 1.
(24) Cheng, S. Z. D.; Cao, M.-Y.; Wunderlich, B. *Macromolecules* **1986**, *19*, 1868.
(25) Cheng, S. Z. D.; Wu, Z.; Wunderlich, B. *Macromolecules* **1987**, *20*, 2802.
(26) Schlosser, E.; Schonhals, A. *Colloid Polym. Sci.* **1989**, *267*, 963.
(27) Schick, C.; Dobbertin, J.; Potter, M.; Dehne, H.; Hensel, A.; Ghoneim, A. M.; Weyer, S. J. *J. Therm. Anal.* **1997**, *49*, 499.
(28) Schick, C.; Wurm, A.; Mohamed, A. *Colloid Polym. Sci.* **2001**, *279*, 800.
(29) Kobayashi, Y.; Zheng, W.; Meyer E. F.; McGervey, J. D.; Jamieson, A. M. *Macromolecules* **1989**, *22*, 2302.
(30) Kluin, J. E.; Yu, Z.; Vleeshouwers, S.; McGervey, J. D.; Jamieson, A. M.; Simha, R. *Macromolecules* **1993**, *26*, 1853.
(31) Cheng, G. W.; Yu, Z.; Jamieson, A. M.; McGervey, J. D. *J. Appl. Polym. Sci.* **1997**, *63*, 483.
(32) Kirkegard, P.; Eldrup, M.; Morgesen, O. E.; Pedersen, N. J. *Comput. Phys. Commun.* **1981**, *23*, 307.
(33) Tao, S. J. *Chem. Phys.* **1972**, *56*, 5499.
(34) Nakanishi, H.; Wang, S. J.; Jean, Y. C. In *Proceedings of the International Conference on Positron Annihilation in Fluids, Arlington, TX*; World Scientific Publishing: Singapore, 1987; p 292.
(35) McCullagh, C. M.; Yu, Z.; Jamieson, A. M.; Blackwell, J.; McGervey, J. D. *Macromolecules* **1995**, *28*, 6100.
(36) Bondi, A. A. In *Physical Properties of Molecular Crystals, Liquids, and Glasses;* Wiley: New York, 1916.
(37) Simha, R.; Carri, G. *J. Polym. Sci., Part B* **1994**, *32*, 2645.

MA034813U